

One galaxy sample to rule them all: HOD modeling of DES Y3 source galaxies

ANDRÉS N. SALCEDO ^{1,2} TIM EIFLER ^{1,2} AND PETER BEHROOZI ^{1,3}

¹*Department of Astronomy/Steward Observatory, University of Arizona, 933 North Cherry Avenue, Tucson, AZ 85721-0065, USA*

²*Department of Physics, University of Arizona, 1118 East Fourth Street, Tucson, AZ 85721, USA*

³*National Astronomical Observatory of Japan, 2-21-1 Osawa, Mitaka, Tokyo, 181-8588, Japan*

ABSTRACT

For the joint analysis of second-order weak lensing and galaxy clustering statistics, so-called 3×2 analyses, the selection and characterization of optimal galaxy samples is a major area of research. One promising choice is to use the same galaxy sample as lenses and sources, which reduces the systematics parameter space that describes uncertainties related to galaxy samples. Such a “lens-equal-source” analysis significantly improves self-calibration of photo-z systematics leading to improved cosmological constraints. With the aim to enable a lens-equal-source analysis on small scales we investigate the halo-galaxy connection of DES-Y3 source galaxies. We develop a technique to construct mock source galaxy populations by matching COSMOS/UltraVISTA photometry onto UNIVERSEMACHINE galaxies. These mocks predict a source halo occupation distribution (HOD) that exhibits significant redshift evolution, non-trivial central incompleteness and galaxy assembly bias. We produce multiple realizations of mock source galaxies drawn from the UNIVERSEMACHINE posterior with added uncertainties in measured DES photometry and galaxy shapes. We fit a modified HOD formalism to these realizations to produce priors on the galaxy-halo connection for cosmological analyses. We additionally train an emulator that predicts this HOD to $\sim 2\%$ accuracy from redshift $z = 0.1 - 1.3$ that models the dependence of this HOD on 1) observational uncertainties in galaxy size and photometry, and 2) uncertainties in the UNIVERSEMACHINE predictions.

Keywords: Cosmology (343), Large-scale structure of the Universe (902), N-body simulations (1083), Galaxy properties (615)

1. INTRODUCTION

Observations of the large-scale structure (LSS) of the Universe contain a wealth of information on fundamental physics questions such as theories of gravity, the mass and number of species of neutrinos, and the nature of dark energy and dark matter. Existing and future galaxy redshift surveys such as the Kilo-Degree Survey (KiDS, [Hildebrandt et al. 2017](#); [Heymans et al. 2021](#)), the Dark Energy Survey (DES, [Abbott et al. 2018](#); [DES Collaboration et al. 2021](#)), the Hyper Suprime-Cam (HSC, [Hikage et al. 2019](#)), the Baryon Oscillation Spectroscopic Survey, the Dark Energy Spectroscopic Instrument (DESI, [DESI Collaboration et al. 2016](#)), the Vera C. Rubin Observatory Legacy Survey of Space and

Time (LSST, [Ivezić et al. 2019](#)), the Nancy Grace Roman Space Telescope ([Akeson et al. 2019](#)), the Euclid ([Laureijs et al. 2011](#)), and the Spectro-Photometer for the History of the Universe, Epoch of Reionization, and Ices Explorer (SPHEREx, [Doré et al. 2014](#)) aim to unlock this information through a variety of imaging and spectroscopic measurements.

One of the main challenges for joint analyses of weak lensing and galaxy clustering observables in ongoing and future surveys is the modeling of small scales. While uncertainties in the non-linear evolution of the matter density field pose a common problem for both lensing and clustering, more significant limitations arise from our lack of understanding of feedback and cooling processes that affect baryons and inadequacies in modeling the galaxy-halo connection. For cosmic shear, which is directly sensitive to the matter distribution, baryonic modeling uncertainties are the main limitation when pushing to small scales. For galaxy clustering

and for galaxy-galaxy lensing, uncertainties in modeling the galaxy-halo connection are the dominant systematic that prohibit the inclusion of small scales.

In the clustering and galaxy-galaxy lensing category a variety of concepts have been proposed to go beyond the galaxy bias description of linear perturbation theory (Kaiser 1984). Higher-order perturbative models for galaxy biasing are an active research area (see Desjacques et al. 2018, for a review) pushing our ability to model galaxy bias into the quasi-linear regime. More recently, this boundary has been pushed to even smaller scales by Hybrid Effective Field Theory models (HEFT), which utilize a combination of analytical bias description and numerical displacements calculated from N-body simulations to describe the statistical distribution of the galaxy density field (Modi et al. 2020; Kokron et al. 2021; Hadzhiyska et al. 2021; Zennaro et al. 2023).

Halo Occupation Distribution (HOD) models fall into the category of empirical models that describe the galaxy-halo connection (e.g. Berlind & Weinberg 2002; Zehavi et al. 2005; van den Bosch et al. 2013). HOD methods statistically specify the relationship between galaxies and their host halos, primarily as a function of host halo mass. These methods enable interpretation of measurements of galaxy-galaxy lensing and galaxy clustering into the fully non-linear regime. This is done at the expense of introducing additional free parameters, but non-linear clustering data can constrain them leading to improved constraints on cosmological parameters (e.g. Yoo et al. 2006; Zheng & Weinberg 2007; Cacciato et al. 2009, 2012, 2013; Leauthaud et al. 2011; Yoo & Seljak 2012; More et al. 2013).

For the design of clustering analyses of future surveys it is necessary to consider the impact of galaxy bias uncertainties on the overall error budget holistically. Statements that a specific galaxy bias parameterization is accurate at a specific %-level up to a specific k are interesting, but insufficient in the context of quantifying the trade space of parameter bias and errors in the posterior probability. When pushing to smaller scales, the hope of smaller confidence intervals is countered by the need for additional model complexity to reduce cosmological parameter biases. Model complexity enters through additional nuisance parameters that open up more degrees of freedom and through increasingly wide priors on the existing nuisance parameters. Both aspects affect not only the small scales that analysts aim to include, unfortunately these parameterizations impact all scales of the analysis. As a consequence the increased model complexity that allows for the inclusion of small scales can result in a degradation of constraining power overall.

The DES Y3 joint analysis of galaxy clustering, galaxy galaxy lensing, and cosmic shear (referred to as 3x2) (Abbott et al. 2022) uses linear galaxy bias with one galaxy bias parameter per tomographic bin. With respect to uncertainties in small scale bias modeling this analysis has been shown to be unbiased with scale-cuts of 6 and 8 h^{-1} Mpc for galaxy-galaxy lensing and clustering, respectively (Krause et al. 2021). The DES Y3 2x2 analysis (Pandey et al. 2022), which only combines galaxy clustering and galaxy-galaxy lensing, explores the inclusion of smaller scales in the analysis at the cost of adding a second parameter per tomographic bin (1-loop perturbation theory) to describe non-linear galaxy bias evolution. As a result this analysis is able to include scales down to 4 and 8 h^{-1} Mpc for clustering and galaxy-galaxy lensing respectively, without incurring cosmological parameter biases. The resulting gain in cosmological information is negligible however, likely due to the increased parameter space.

A corresponding analysis from the HSC collaboration using CMASS galaxies as the lens sample and HSC galaxies as sources is presented in (Sugiyama et al. 2023; Miyatake et al. 2023). The first analysis relies on perturbation theory to push to smaller scales and the latter uses an HOD model of CMASS galaxies (More et al. 2015). Miyatake et al. (2022) use 4 different variations of this HOD to populate numerical simulations, generate corresponding mock catalogs, and show that their pipeline can recover the input cosmology robustly given wide priors on the HOD parameters.

The main goal of this paper is to derive an HOD model for the DES Y3 source sample that includes realistic, informative priors on the HOD parameters. Following Schaan et al. (2020); Fang et al. (2022) this will enable future joint analyses of e.g. galaxy clustering, weak lensing, CMB lensing and their cross-correlations using only the source galaxy sample without the need to characterize a separate lens or clustering sample. This “lens-equal-source” approach is to reduce the systematics parameter space, in particular regarding photo- z parameters, and to improve self-calibration of other systematic effects.

The source sample HOD is obtained via a matching process utilizing UNIVERSEMACHINE (Behroozi et al. 2019) mock data and COSMOS/UltraVISTA photometry (Muzzin et al. 2013a). This process is used to generate mock catalogs of DES galaxy imaging, we then apply DES-Y3 source selection criteria and measure the resulting HOD. We subsequently vary the input parameters to our machinery (colors, magnitudes, sizes) to determine uncertainties in the source HOD, which can be used as priors in future analyses.

The paper is structured as follows: In Section 2 we describe the construction of our DES Y3 mock catalogs, that lead to the construction of the HOD in Section 3 where we also characterize the uncertainties in our mock construction process. We derive priors on the relevant parameters in Section 4 and conclude in Section 5 .

2. CONSTRUCTING MOCKS OF DES GALAXY IMAGING

2.1. Source galaxy selection in Dark Energy Survey Year 3 data

The parent sample for the DES-Y3 source sample (Gatti et al. 2021) is the DES-Y3 GOLD catalog (GOLD catalog from here on). The GOLD catalog comprises 326,049,983 objects over $\sim 4143 \text{ deg}^2$ of sky with observations in the *griz* bands. The METACALIBRATION algorithm (Sheldon & Huff 2017; Huff & Mandelbaum 2017) was applied to this catalog using *riz*¹ bands to produce a shape catalog from which the source sample was selected.

To construct the source galaxy catalog the following selections were applied to the GOLD catalog,

1. Any objects outside of the unmasked regions of the GOLD catalog and flagged as “anomalous” are removed.
2. A signal-to-noise cut of $10 < \text{S/N} < 1000$ is applied. The low end of this cut removes faint objects impacted by detection biases while the high end removes very bright objects for which Poisson noise could be dominant relative to typical background noise.
3. A PSF-size-ratio cut is applied, $T/T_{\text{PSF}} > 0.5$, where,

$$T = I_{xx} + I_{yy}, \quad (1)$$

referred to as the galaxy size in this context, is the sum of second moments of the Gaussian-model surface brightness profile,

$$I_{\mu\nu} = \frac{\int dx dy I(\mu, \nu) (\mu - \bar{\mu})(\nu - \bar{\nu})}{\int dx dy I(\mu, \nu)}. \quad (2)$$

The sizes used are averaged from all exposures and bands.

4. A further size cut of $T < 10 \text{ arcsec}^2$ is applied to remove the largest objects. Visual inspection

found that most of the objects cut are not themselves large but have their size estimate affected by large neighbors.

5. Objects with $T > 2 \text{ arcsec}^2$ and $\text{S/N} < 30$ are also cut. These objects are relatively large and faint and are mostly blended upon visual inspection.
6. Color and magnitude cuts are applied to limit objects to those with the best photometric redshifts. These cuts are,

$$18 < i < 23.5, \quad (3)$$

$$15 < r < 26, \quad (4)$$

$$15 < z < 26, \quad (5)$$

$$-1.5 < r - i < 4, \quad (6)$$

$$-1.5 < z - i < 4. \quad (7)$$

7. A final selection was made to limit binary-star contamination. For high ellipticity objects ($|e| > 0.8$) a cut is made in r - T space,

$$\log_{10}(T/\text{arcsec}^2) < (22.5 - r)/2.5. \quad (8)$$

The number of objects that pass this selection is 100,204,026. While a large fraction of GOLD catalog objects fail the various S/N criteria only a relatively small fraction ($\sim 6\%$) require *only* S/N information to be excluded, i.e. are not also removed by a cut on magnitude, color, or size.

2.2. UNIVERSEMACHINE galaxies

The UNIVERSEMACHINE algorithm (Behroozi et al. 2019) models the connection between galaxy and halo assembly by parametrizing galaxy star formation rates (SFRs) as a function of halo potential well depth (specifically the maximum circular velocity at the time of peak halo mass, $v_{\text{max}}(z_{M_{\text{peak}}})$, redshift and assembly history with a total of 44 free model parameters. This parametrization is constrained by a variety of observational data: observed stellar mass functions, SFRs, quenched fractions, UV luminosity functions, UV-stellar mass relations, IRX-UV relations, projected auto- and cross-correlation functions, and the dependence of quenching fraction on environment. The output of this algorithm is a catalog of mock galaxies with realistic SFRs, stellar masses, and UV-luminosities as well as host subhalo properties.

In what follows we utilize publically available UNIVERSEMACHINE catalogs² built on the Small Multi-Dark Planck (SMDPL) and Bolshoi-Planck simulations

¹ The *g*-band was omitted due to known issues with PSF estimation

² <https://www.peterbehroozi.com/data.html>

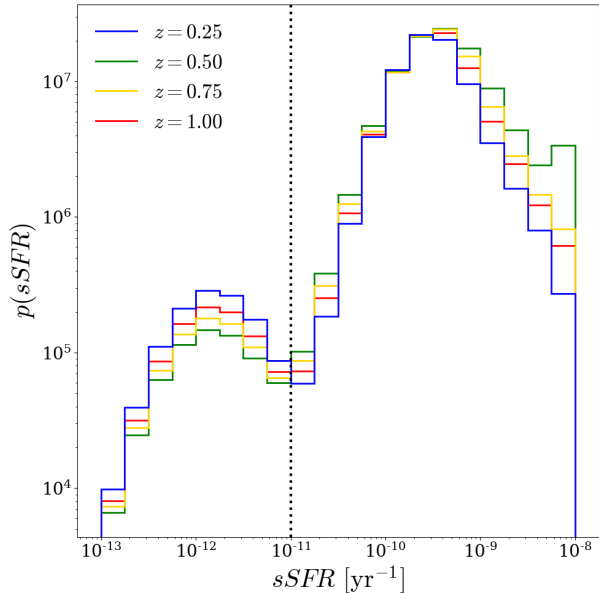


Figure 1. Distribution of specific-SFR (sSFR) in the SMDPL UNIVERSEMACHINE mock galaxy catalog at $z = 0.25$ (blue), $z = 0.50$ (green), $z = 0.75$ (yellow), and $z = 1.0$ (red). The dotted vertical line at $sSFR = 10^{-11} \text{ yr}^{-1}$ located at a local minimum in the distribution divides galaxies into star-forming and quiescent. We observe that the location of this minimum is insensitive to redshift.

(Klypin et al. 2016).³ Both are dark-matter-only cosmological N-body simulations in periodic cubes, with particle resolution of $M_{\text{part}} \sim 1-2 \times 10^8 h^{-1} M_{\odot}$, sufficient to resolve the host halos of DESY3 source galaxies. The SMDPL cube has side length $L_{\text{side}} = 400 h^{-1} \text{ Mpc}$ while Bolshoi-Planck has side length $L_{\text{side}} = 250 h^{-1} \text{ Mpc}$. The SMDPL cosmology is based on the Planck Collaboration et al. (2016) results with $\Omega_m = 0.307$, $\Omega_{\Lambda} = 0.692$, $\sigma_8 = 0.823$ and $h = 0.678$. The Bolshoi-Planck cosmology is the same with the exception of $h = 0.70$. In what follows we use virial halo masses M_{vir} based on the redshift-dependent spherical overdensity definition of Bryan & Norman (1998). Fig. 1 shows the specific star-formation rate (sSFR) distribution at $z = 0.5$ and $z = 1.0$ within these catalogs. We see at both low- and high-redshift a clear splitting into a quiescent and star-forming population at $sSFR = 10^{-11} \text{ yr}^{-1}$.

2.3. COSMOS/UltraVISTA galaxy catalog

We use the public K_s -selected catalog COSMOS/UltraVISTA catalog of Muzzin et al. (2013a) to assign colors to our mock galaxies. This catalog aggregates photometric data taken in the COS-

MOS/UltraVISTA field. Far to near UV imaging was provided by the *Galaxy Evolution Explorer* satellite (GALEX; Martin et al. 2005), optical broad to medium band imaging from the Canada-France-Hawaii Telescope (CFHT; Capak et al. 2007), near-infrared data from the UltraVISTA survey (McCracken et al. 2012), and mid-infrared data from *Spitzer* (Sanders et al. 2007). Galaxies are identified in this data and those with $K_s > 24.35$ are kept in the catalog. The resulting catalog covers 1.62 deg^2 of the sky and provides photometry in 30 bands (covering a wavelength range of $0.15-24 \mu\text{m}$) for 262,615 galaxies.

Muzzin et al. (2013a) provide photometric redshifts calculated using the EAZY software (Brammer et al. 2008). Based on spectroscopic overlap these photometric redshifts are reliable at $z_{\text{spec}} < 1.5$ with an error of $\delta z/(1+z) = 0.013$, with a 1.56% outlier fraction ($> 3\sigma$ from the mean relation). Muzzin et al. (2013a) also provide estimates of stellar mass and SFR obtained from SED fits using either models from Bruzual & Charlot (2003) or models from Maraston (2005). In what follows we will use stellar masses and SFR based on the Maraston (2005) models, though we have checked that this choice has no qualitative impact on our results.

2.4. Matching UNIVERSEMACHINE and COSMOS/UltraVISTA galaxies

To obtain insight into the form of the DES source galaxy HOD we match COSMOS/UltraVISTA photometry and assign intrinsic galaxy sizes to UNIVERSEMACHINE galaxies. In the case of both COSMOS/UltraVISTA and UNIVERSEMACHINE we rely on splitting galaxies into star-forming and quiescent populations. In UNIVERSEMACHINE this is accomplished by applying a cut at $sSFR = 10^{-11} \text{ yr}^{-1}$ as shown in Fig. 1. For the COSMOS/UltraVISTA galaxies we rely on the well-known bimodality in color-color (rest frame $U - V$ vs. $V - J$) space to differentiate between star-forming and quiescent galaxies. Figure 2 plots $U - V$ versus $V - J$ for COSMOS/UltraVISTA galaxies in four redshift bins. Points represent a subsample of the galaxies in each bin colored red (quiescent) or blue (star-forming) based on sSFR calculated from the SFRs and stellar masses reported by Muzzin et al. (2013a). We observe a clear bimodality in all redshift bins with low and high sSFR galaxies cleanly separated in color-color space. We also plot solid black lines (Muzzin et al. 2013b) that we use to tag galaxies as either quiescent or star-forming.

³ <https://www.cosmosim.org/cms/simulations/smdpl/>

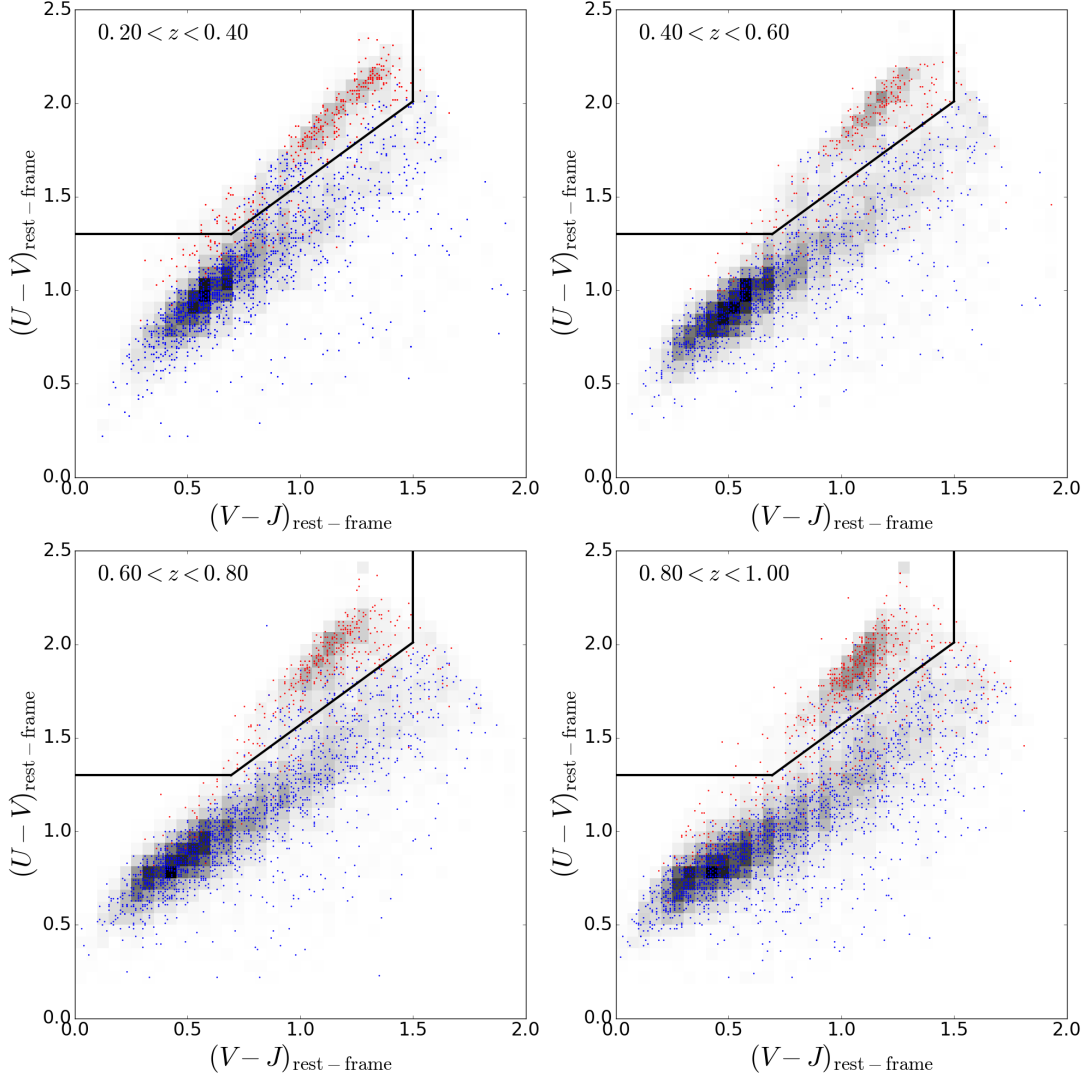


Figure 2. Color-color diagrams for COSMOS/UltraVISTA galaxies binned by redshift. Black lines divide the the galaxies into quiescent (upper region) and star-forming (lower region) population. A subsample of the galaxies are plotted as points that are colored red (quiescent, $\text{sSFR} < 10^{-11} \text{ yr}^{-1}$) or blue (star-forming, $\text{sSFR} > 10^{-11} \text{ yr}^{-1}$) based on the COSMOS/UltraVista estimated sSFR. We observe acceptable agreement between the quiescent/star-forming separation using color information and estimated sSFR.

Quiescent galaxies are defined as,

$$U - V > 1.3 \text{ and } V - J < 1.5, \text{ for all } z, \quad (9)$$

$$U - V > 0.88(V - J) + 0.69, \text{ for } 0.0 < z < 1.0, \quad (10)$$

$$U - V > 0.88(V - J) + 0.59, \text{ for } 1.0 < z < 3.0, \quad (11)$$

with star-forming galaxies making up the remaining population. These cuts were originally defined by Williams et al. (2009) to maximize the difference in specific star formation rates between the two populations and have since been adjusted by Muzzin et al. (2013a) to account for the difference in UltraVISTA rest-frame color distributions.

To match COSMOS/UltraVISTA photometry to a redshift snapshot of UNIVERSEMACHINE galaxies we use the following procedure:

1. Select COSMOS/UltraVISTA galaxies in the range $z_{\text{UM}} - 0.05 < z_{\text{phot}} < z_{\text{UM}} + 0.05$, where z_{UM} is the redshift of the relevant UNIVERSEMACHINE catalog and z_{phot} is the photometrically estimated redshift for each COSMOS/UltraVISTA galaxy.
2. Separate mock and data galaxies into quiescent and star-forming populations as described above. In the case of UNIVERSEMACHINE this is done directly with the sSFR. In the case of COS-

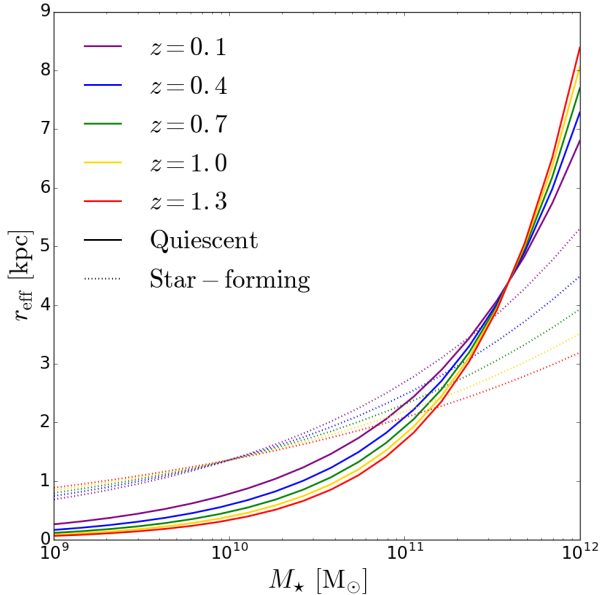


Figure 3. Redshift dependent size-mass relations from Mowla et al. (2019b). There are separate relations for quiescent (solid-line) and star-forming (dashed-line) galaxies that evolve significantly with redshift, and cross over each other at high stellar mass.

MOS/UltraVISTA galaxies this separation is determined in rest-frame color-color space.

3. Finally for each UNIVERSEMACHINE galaxy we assign the photometry (i.e. i -, r -, z -band magnitudes) of the COSMOS/UltraVISTA galaxies that is closest in stellar mass and of the same population (quiescent/star-forming).

We also assign sizes using the size-stellar mass relations of Mowla et al. (2019b)⁴ for galaxies $z < 3$ calibrated from COSMOS-DASH and 3D-HST/CANDELS data. Mowla et al. (2019b) provide separate redshift-dependent relations for star-forming and quiescent galaxies of the form

$$r_{\text{eff}}(m_*)/\text{kpc} = A \times m_*^\alpha, \quad (12)$$

$$m_* = M_*/(7 \times 10^{10} M_\odot), \quad (13)$$

⁴ See also van der Wel et al. (2014); Mowla et al. (2019a)

where r_{eff} is effective radius, the semi-major axis of the ellipse containing half the flux of the galaxy, and

$$\log A = \begin{cases} -0.29 \log(1+z) + 0.91 & \text{star-forming,} \\ -0.54 \log(1+z) + 0.72 & \text{quiescent,} \end{cases} \quad (14)$$

$$\alpha = \begin{cases} -0.15 \log(1+z) + 0.31 & \text{star-forming,} \\ 0.31 \log(1+z) + 0.44 & \text{quiescent.} \end{cases} \quad (15)$$

Figure 3 shows these relations over a range of redshifts. Both quiescent and star-forming galaxies increase in size with increasing stellar mass. The relation of size and redshift is non-monotonic reversing for high-mass ($M_* > 4 \times 10^{11} M_\odot$) quiescent and low-mass ($M_* < 10^{10} M_\odot$) star-forming galaxies. At low stellar masses star-forming galaxies tend to be larger than their quiescent counterparts. This trend reverses between $M_* \approx 1\text{-}2 \times 10^{11} M_\odot$ depending on galaxy redshift.

In addition to the mean of these relations we also consider the scatter in r_{eff} at fixed stellar mass denoted $\sigma_{\log r_{\text{eff}}}$. Mowla et al. (2019a) report this scatter to be roughly log-normal and constant in stellar mass with values ranging between 0.2 and 0.3 dex for both quiescent and star-forming galaxies. They also report minimal redshift evolution of this quantity. These results are in good agreement with others from the literature (Ichikawa et al. 2012; van der Wel et al. 2014). Therefore we will adopt a constant lognormal scatter with respect to stellar mass and redshift with value $\sigma_{\log r_{\text{eff}}} = 0.25$ as our fiducial model of size-mass scatter.

To apply the source galaxy selection criteria we must convert r_{eff} into the size T (described in detail in Section 2.1). Assuming a circular two-dimensional Gaussian intensity profile for source galaxies and relating its second moments to the half-light radius r_{eff} yields,

$$T = \frac{r_{\text{eff}}^2}{\left[\text{erf}^{-1}\left(\frac{1}{\sqrt{2}}\right)\right]^2}, \quad (16)$$

which we convert into angular units using the redshift of each of our simulation snapshots. For our star-forming galaxies we additionally randomly incline them with respect to the line-of-sight when computing their apparent size.

3. MODELING THE HOD OF DES SOURCE GALAXIES

3.1. Applying source galaxy selection to mock galaxies

With COSMOS/UltraVISTA photometry matched to UNIVERSEMACHINE galaxies and sizes assigned we can

apply the DES-Y3 source selection criteria to our mock galaxies and directly measure their HOD. The selection criteria are described in detail in Section 2.1 and summarized here,

$$18 < i < 23.5, \quad (17)$$

$$15 < r < 26, \quad (18)$$

$$15 < z < 26, \quad (19)$$

$$-1.5 < r - i < 4, \quad (20)$$

$$-1.5 < z - i < 4, \quad (21)$$

$$\frac{T_{\text{PSF}}}{2} < T < 10 \text{ arcsec}^2, \quad (22)$$

where $T_{\text{PSF}} = 0.33 \text{ arcsec}^2$ is the average for DESY3 data source galaxies. The left-hand panel of Fig. 4 shows the predicted source galaxy HOD over a range of redshifts for centrals (red), satellites (blue), and all galaxies (black).

We plot the mass-dependence of the HOD in terms of the characteristic collapse mass M_c satisfying $\sigma(M_c(z)) = \delta_c$ where $\sigma(M, z)$ is the square root of the variance in the linear density field and $\delta_c = 1.686$ is the threshold linear overdensity for spherical collapse. Across redshifts we see that the central occupation is roughly consistent with the standard form, i.e. an error-function, albeit with significant incompleteness.

We find that the central occupation does not converge to a single value with increasing mass at any redshift, though it is difficult to distinguish between genuine mass-dependent behavior and noise. In either case the contribution to the galaxy bias from high mass halos will be dominated by the satellite term. We also see that the level of central incompleteness is dependent on redshift, roughly 60–70% halos host a central at $z = 0.50$, with this fraction decreasing to roughly 40% at $z = 1.0$. However, this behavior is not monotonic across the entire redshift range we consider, at $z = 0.25$ we see a precipitous decline in high-mass occupation driven by the large size cut, $T < 10 \text{ arcsec}^2$.

In the case of the satellites we see that at all redshifts the satellite occupation takes the familiar form of a power-law with an exponential cut-off at low masses. We observe that the cut-off mass and the characteristic mass to host a satellite depend on redshift and that both increase with increasing redshift. In contrast the slope of the satellite-occupation power law only evolves negligibly with redshift.

In the right-hand panel of Fig. 4 we investigate the impact of the selection criteria at $z = 1.0$. Dot-dashed curves show the impact of relaxing our magnitude cuts (equations 17-19), dashed curves show the impact of relaxing the color cuts (equations 20 and 21), and dotted

curves show the impact of relaxing the size cuts (equation 22). We see that both our magnitude and size cuts significantly change the normalization of the satellite occupation but have less of an effect on the slope. The color cuts have negligible impact on the satellite occupation, indicating that they are redundant with the magnitude and size cuts.

The impact on the central term is more complicated. We see that the degree and form of the observed incompleteness is driven by our size cut, i.e. when the size cut is relaxed we obtain a standard error-function form for our central occupation. This effect is ultimately a result of a complex interplay between the stellar-to-halo mass relation, the quenched fraction and the size-stellar mass relations for star-forming and quiescent galaxies. In Fig. 3 we see that the quiescent size-mass relation crosses over the star-forming relation at large stellar mass. Similarly the quenched fraction evolves with stellar/halo mass. The redshift evolution of this behavior observed in the right-hand panel of Fig. 4 becomes more complicated as the large and small size cuts are fixed in angular size and therefore correspond to different physical sizes at different redshifts.

At the low mass end we see that the occupation is most affected by our magnitude cuts, which remove low magnitude galaxies hosted by low mass halos. When the magnitude cuts are relaxed the characteristic mass to host a central decreases by almost an entire dex. Additionally we see that the magnitude cuts largely determine the scatter in the characteristic mass to host a central. When these are relaxed the width in the transition from zero occupation is broadened significantly. As in the case of the satellite occupation we see that the color cuts are almost entirely redundant with the size and magnitude cuts.

3.2. Analytic HOD parameterization

In Fig. 4 we have shown the HOD of mock source galaxies in our UNIVERSEMACHINE-COSMOS/UltraVISTA matched catalog. Across a wide redshift range we observe a power-law satellite term consistent with a standard HOD parameterization. The central term exhibits significant incompleteness with complex mass-dependence. Fortunately, the more complicated features of this incompleteness occur at high mass where the central contribution to the galaxy correlation function is small relative to that from the satellite term. Therefore we adopt a modified version of the standard HOD parameterization (e.g. Berlind & Weinberg 2002; Zheng et al. 2005) for the source central and satellite occupations as a fully analytic option for modeling

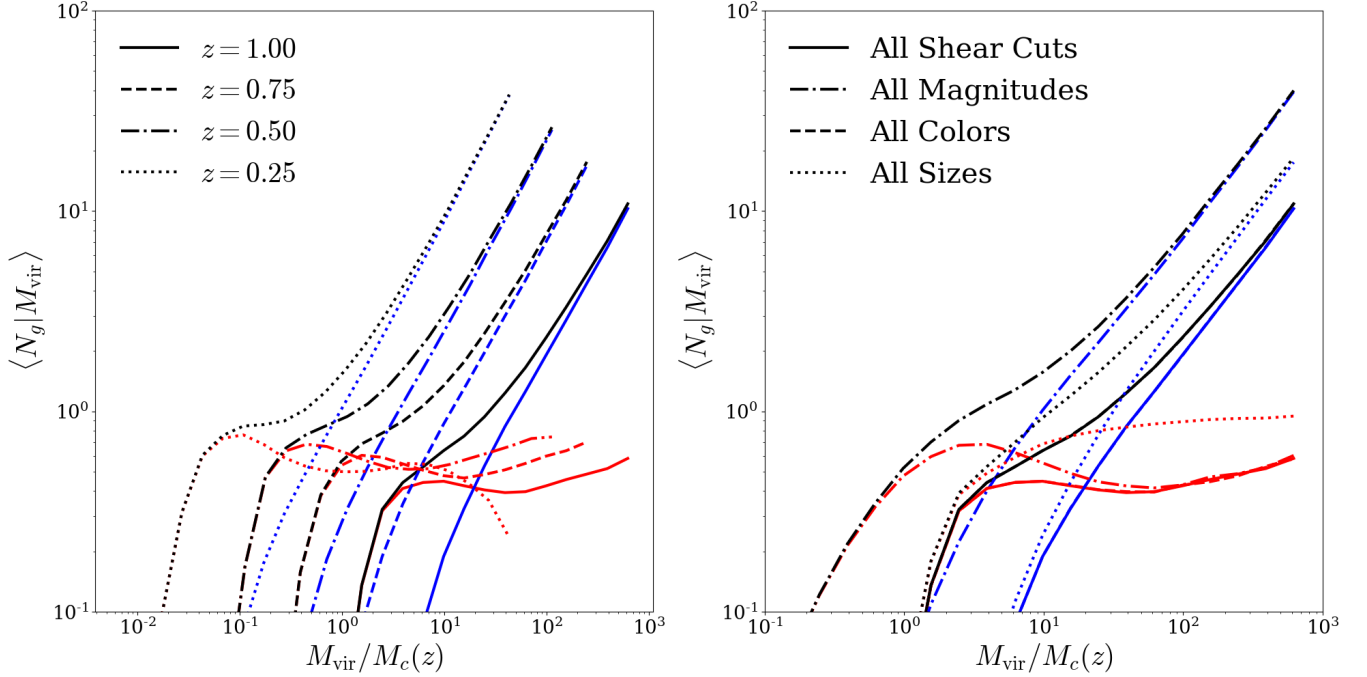


Figure 4. The HOD of UNIVERSEMACHINE-COSMOS/UltraVISTA matched source galaxies for central (red), satellite (blue) and all (black) galaxies. The left-hand panel shows how the source HOD varies with redshift. We observe significant redshift evolution in the range $z = 0.25 - 1.00$, particularly in the characteristic mass scales to host centrals and satellites. The right-hand panel shows the effect of relaxing selection criteria at $z = 1.00$. The solid line shows the HOD obtained with all selection criteria applied, the dot-dashed curves show the impact of relaxing the magnitude cuts, the dashed shows the impact of relaxing color cuts, and the dotted shows the impact of relaxing size cuts. We see that the significant central-incompleteness we observe is driven by cuts on galaxy size (see text).

the DES-Y3 source sample HOD,

$$\langle N_{\text{cen}} | M_h \rangle = \frac{f_{\text{cen}}(M)}{2} \left[1 + \text{erf} \left(\frac{\log M - \log M_{\text{min}}}{\sigma_{\log M}} \right) \right] \quad (23)$$

$$\langle N_{\text{sat}} | M_h \rangle = \frac{\langle N_{\text{cen}} | M_h \rangle}{f_{\text{cen}}(M)} \left(\frac{M}{M_1} \right)^\alpha \quad (24)$$

$$f_{\text{cen}}(M) = \min \left[f_{\text{cen},0} \left(1 + \frac{M}{10^{\log M_{\text{min}} + \sigma_{\log M}}} \right)^\beta, 1.0 \right] \quad (25)$$

where the familiar parameter M_{min} represents the characteristic halo mass required to host a central ($\langle N_{\text{cen}} | M_{\text{min}} \rangle = 0.5$), the parameter $\sigma_{\log M}$ determines the sharpness of the transition from $\langle N_{\text{cen}} \rangle = 0.0$ to $\langle N_{\text{cen}} \rangle = 1.0$, M_1 is the characteristic halo mass required to host a satellite ($\langle N_{\text{cen}} | M_{\text{min}} \rangle = 1.0$), and α is the slope of the satellite power law. We also include a linear mass-dependent incompleteness term characterized by $f_{\text{cen}}(M)$, with normalization $f_{\text{cen},0}$ and slope β . This is to model the nontrivial central incompleteness which we observe in Fig. 4.

Figure 5 shows the result of fitting this parameterization to our fiducial source HODs at redshifts $z = 0.25$,

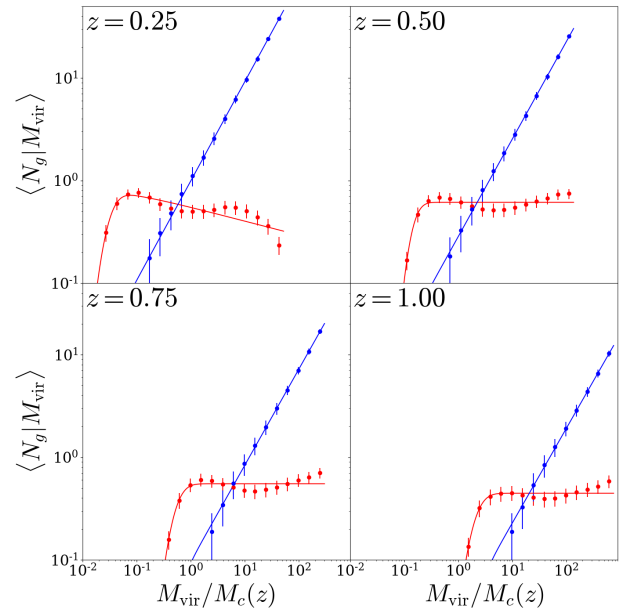


Figure 5. Best fitting HOD models for our mock source galaxies at $z = 0.25$ (top-left), $z = 0.50$ (top-right), $z = 0.75$ (bottom-left), and $z = 1.00$ (bottom right). We see that the satellite term is very well fit by a standard power law, while the modified central term captures overall changes in incompleteness as a function of mass.

0.50, 0.75 and 1.00. This fitting is done by minimizing the χ^2 for the central and satellite terms separately in each redshift bin. We see that across our redshift range the satellite occupation is well fit by a standard power-law occupation. The overall mass dependence of the observed central incompleteness is described by our parameterization. At high masses we see some degree of model mis-specification but in this mass regime the satellite occupation dominates the HOD and galaxy bias.

4. HOD PRIORS FOR COSMOLOGICAL ANALYSES

4.1. HOD sensitivity to underlying assumptions

Thus far we have obtained results for the DES-Y3 source HOD assuming a single realization the UNIVERSEMACHINE algorithm, a single fiducial value for the scatter in the size-mass relation, and we have ignored the potential for the source sample to exhibit galaxy assembly bias. In Fig. 6 we examine the impact of each of these assumptions on our results.

Beginning with the top-panel we test the impact of UNIVERSEMACHINE uncertainties on our HOD results. The UNIVERSEMACHINE fits a variety of galaxy observational data using a 44-parameter forward modeling framework that parameterizes galaxy star formation rate as a function of host halo properties. Our matching scheme relies on the specific star formation rates and stellar masses of galaxies that this forward model predicts and is therefore sensitive to uncertainties in these model parameters.

To quantify this we draw 100 realizations from the UNIVERSEMACHINE posterior and apply these model realizations to the Bolshoi-Planck simulation. For each of these 100 realizations we then recalculate the expected source HOD. The top-panel of Fig. 6 shows the result of this test at redshift $z = 0.25, 0.50, 0.75,$ and 1.00 . Solid lines show the mean total HOD occupation, while dashed lines show the central component and dotted lines show the satellite component. The colored bands show the $1-\sigma$ error from our 100 realizations. When propagated through our matching scheme the uncertainty of the HOD on the UNIVERSEMACHINE posterior is at the 3–5% percent level. The resulting uncertainty on the satellite fraction is 4 – 5%. We will further quantify the level of this variation in the context of producing HOD-priors for cosmological analyses in subsequent sections.

In the middle-panel of Fig. 6 we investigate the impact of scatter in the size-mass relation on the HOD. For satellites increasing the scatter reduces the occupation at all masses. For centrals the impact of changing the scatter is mass-dependent. At low and high masses in-

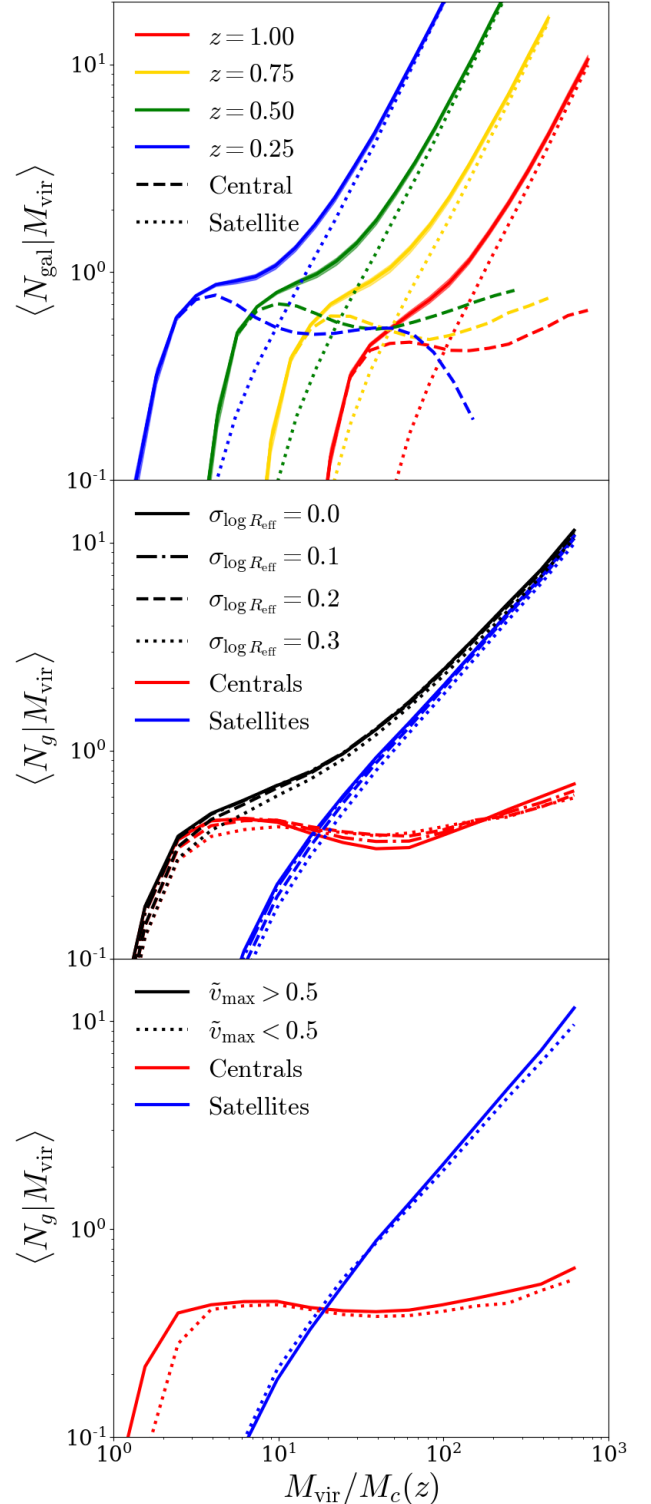


Figure 6. Robustness tests for our UNIVERSEMACHINE-based source HOD results described in Section 4.1. The top-panel shows the error on our fiducial HOD due to UNIVERSEMACHINE uncertainties across the redshift range we consider. The middle-panel shows the impact of the variations in the assumed scatter in the size-mass relation. Finally the bottom-panel shows the level of galaxy assembly bias we observe in our mocks.

creased scatter decreases the occupation due to the small and large size cuts. Meanwhile in an intermediate mass range increased scatter increases the occupation. This mass-dependent behavior tends to flatten out the central occupation, which has the deepest local minimum at intermediate masses in the case of no scatter. The detailed features of the observed central incompleteness are due to the small and large size cuts used to select source galaxies, as the scatter increases and tends to dominate over the mean size-mass relation these features become less salient and the central occupation is flattened.

Finally in the bottom-panel of Fig. 6 we investigate the level of galaxy assembly bias present in the source sample. Galaxy assembly bias refers to the possibility for galaxy occupation to depend on properties other than mass,

$$\langle N|M_h \rangle \neq \langle N|M_h, S \rangle, \quad (26)$$

where S is some secondary property (e.g. Croton et al. 2007; Zu et al. 2008; Zentner et al. 2014; McCarthy et al. 2019; Zentner et al. 2019; Salcedo et al. 2022; Wang et al. 2022). If there also exists a halo assembly bias (e.g. Sheth & Tormen 2004; Gao et al. 2005; Harker et al. 2006; Wechsler et al. 2006; Gao & White 2007; Jing et al. 2007; Wang et al. 2007; Li et al. 2008; Faltenbacher & White 2010; Mao et al. 2018; Salcedo et al. 2018; Sato-Polito et al. 2019; Xu & Zheng 2018; Johnson et al. 2019) signal with respect to the same property then the galaxy bias will differ from that predicted by a standard HOD model.

In the case of both centrals and satellites we compute the mean occupation for haloes with maximum circular velocity v_{\max} greater (solid) and less (dotted) than the median for haloes of that mass. We see that the haloes with high v_{\max} for their mass are more likely to host central galaxies, particularly at low masses. In contrast the satellite occupation is not significantly affected by v_{\max} . This is a clear indication of galaxy assembly bias in our mock source galaxy sample that must be properly marginalized over to produce robust cosmological constraints.

4.2. Analytic HOD priors for cosmological analysis

By matching COSMOS/UltraVISTA photometry to UNIVERSEMACHINE mock galaxies we have constructed mock galaxy catalogs with the properties necessary to apply DES-Y3 source galaxy selection criteria in order to study their galaxy-halo connection and develop an HOD model for future cosmological analyses. As discussed in Section 4.1 our best-fit HOD is sensitive to variations in the underlying parameters. Our framework allows us to quantify these uncertainties to obtain priors that can be used in future cosmological analyses.

To produce such priors we must propagate the systematic uncertainties in our matching scheme to uncertainties on HOD parameters. The main sources of systematic uncertainties in this process are,

- Uncertainty in the relation between COSMOS/UltraVISTA and DES photometry.
- Posterior uncertainties on the UNIVERSEMACHINE model parameters
- Uncertainties in the galaxy size-stellar mass relation.

In each case we can make reasonable assumptions about the level of uncertainty, and therefore we can convert these assumptions into priors on HOD parameters.

To do this we generate noisy and biased realizations of our fiducial DES source selection. We use the 100 draws from the UNIVERSEMACHINE posterior applied to the Bolshoi-Planck simulation described in Section 4.1. We additionally treat the bias and gaussian scatter in each of T , i , r , and z as parameters. For these 8 parameters we Latin-hypercube sample over conservative ranges informed by the expected errors in DES photometry and range in galaxy size-stellar mass relations reported in the literature. To each UNIVERSEMACHINE realization we assign 10 sets of bias and scatter parameters and recompute the source HOD for each. This process generates a total of 1000 realizations of the DES source HOD at each of our redshift snapshots.

The variation in resulting HOD relations at a given redshift is therefore representative of our uncertainty on the underlying quantities that impact DES source selection. We fit the central and satellite term of each of these HOD realizations with the parametrization presented in Section 3.2. The mean and standard deviation of the fitted HOD parameters are reported in Table 1 and will serve as the basis for priors in a future HOD analysis of the DES source galaxies.

4.3. Non-parametric emulation of the HOD

An alternative method to model the source HOD and specify priors for a future analysis is to non-parametrically emulate the HOD in terms of the uncertainties described above. Priors in these uncertainties can then be converted into priors on the overall source HOD, and by non-parametrically emulating the HOD we reduce the impact of model mis-specification. Because the UNIVERSEMACHINE has 44 model parameters it is difficult to emulate the entire parameter space, and additionally it is not clear how to set priors on each of these parameters. The most important quantity for our matching scheme that UNIVERSEMACHINE predicts is

Table 1. Mean best fitting HOD parameters and dispersion from the 1000 UNIVERSEMACHINE, scatter and bias realizations.

z	$\sigma_{\log M}$	$\log(M_{\min}/M_c)$	$\log(M_1/M_c)$	α	$f_{\text{cen},0}$	β
0.25	0.41 ± 0.03	-1.51 ± 0.03	-0.02 ± 0.03	0.96 ± 0.01	0.80 ± 0.05	-0.16 ± 0.02
0.50	0.26 ± 0.04	-0.87 ± 0.04	0.55 ± 0.03	0.95 ± 0.02	0.65 ± 0.06	0.03 ± 0.13
0.75	0.25 ± 0.02	-0.31 ± 0.03	1.10 ± 0.04	0.94 ± 0.03	0.57 ± 0.04	0.02 ± 0.11
1.00	0.28 ± 0.05	0.31 ± 0.05	1.73 ± 0.04	0.95 ± 0.04	0.48 ± 0.03	0.03 ± 0.24
1.25	0.38 ± 0.04	1.03 ± 0.10	2.74 ± 0.23	1.01 ± 0.18	0.23 ± 0.04	-0.07 ± 0.19

the stellar mass function, and therefore we will focus on the deviation from the fiducial stellar mass function as our main criterion.

We generate a set of realizations using a similar process to that described above. Instead of generating full UNIVERSEMACHINE realizations we treat the deviation from the fiducial stellar mass function in units of posterior standard deviation σ as a parameter that we Latin-hypercube sample in addition to the scatter and bias in T , i , r and z . We generate 1000 such parameter samples and assign 50 to each of 20 redshift snapshots in the range $z = 0.10 - 1.26$. For each of the 1000 mock realizations we then compute the source HOD.

To emulate this HOD in terms of our parameters and redshift we perform a Gaussian process regression with a squared-exponential kernel in each mass bin of $\langle N_{\text{cen}}|M_{\text{vir}} \rangle$ and $\langle N_{\text{sat}}|M_{\text{vir}} \rangle$. The advantage of this procedure is two-fold, 1) it does not assume an analytic form of the HOD or its redshift evolution and therefore can capture the complex behavior we observe in Fig. 4 and 2) it connects the HOD to observational properties that we can directly place informative priors on. Note that we emulate in bins of M_{vir} rather than M_{vir}/M_c .

Figure 7 shows the results of this emulation. In the top panel we show the set of HOD realizations used to train our emulator split into central (red) and satellite (blue) contributions). In the bottom panel we plot the 1σ leave-one-out error and the bias in our emulation as a function of mass for our central and satellite data. In both cases we see that over the relevant range in halo mass we achieve 1 – 3% errors and are unbiased. In a future cosmological analysis this emulator can be used to directly model and constrain the source HOD.

4.4. Robustness to cosmology

The results presented thus far have been based on a single cosmology used to generate the SMDPL and Bolshoi-Planck simulations. This raises two questions, whether the form of the source HOD depends on cosmology and the extent to which the priors on the HOD we have derived are cosmology dependent. In an HOD context the key quantities to predict galaxy summary statistics are the halo mass function $\frac{dn}{dM_h}$, the halo bias b_h , and the HOD itself $\langle N_g|M_h \rangle$. For example the large

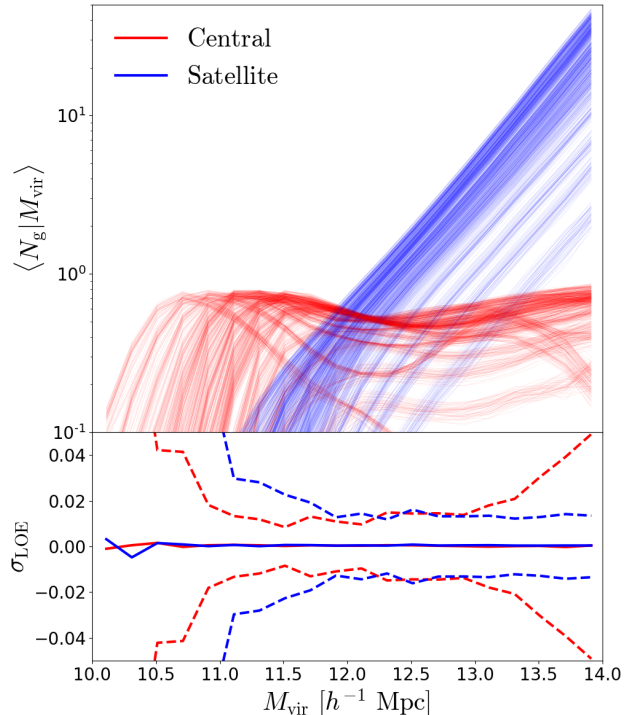


Figure 7. Training samples (top-panel) and leave-one-out emulation errors and biases (bottom-panel) for the central (red) and satellite (blue) contributions to our source HOD. The top panel plots the central and satellite term for each of our 1000 training samples drawn from a wide range of redshifts and observational error models. The bottom panel shows the leave-one-out 1σ error (dashed) and bias (solid) of our emulation as a function of host halo mass.

scale galaxy bias is given by

$$b_g = \frac{1}{n_g} \int dM_h \frac{dn}{dM_h} b(M_h) \langle N_g|M_h \rangle, \quad (27)$$

which is an HOD and halo-mass function weighted sum of the halo bias where n_g is the galaxy number density. Therefore cosmology can affect galaxy formation solely through the halo mass function or halo bias, each of which are easily modeled given current prescriptions. This introduces degeneracies between cosmological and HOD parameters in an analysis of galaxy clustering without any dependence of the HOD on cosmology.

More complicated is the possibility for cosmology to impact the galaxy HOD itself. Previous literature on the

cosmological dependence of galaxy formation has not typically separated these effects. To put the question differently, for a given halo mass at a given redshift how do the galaxy populations formed in such halos depend on cosmology?

Galaxy formation is the complicated product of a variety of physical processes (e.g. Somerville & Davé 2015) many of which are not yet fully understood and not resolvable in cosmological hydrodynamic simulations. In the standard picture, every galaxy is formed within a halo with initial properties associated with its host’s mass and accretion history. In addition to forming a central galaxy at their center, halos acquire new galaxies through mergers with other halos. The orbits of the newly acquired satellites will gradually decay and lead to interactions and mergers with the central. The standard HOD formalism assumes that the outcome of this linked halo and galaxy formation process depends only on host halo mass. If this assumption holds then the key ingredients to predict the HOD at a given redshift are the stellar-to-halo mass relation (SHMR) and the subhalo mass function. The degeneracy between redshift and cosmological parameters is mostly accounted for by considering the HOD in units of the redshift- and cosmology-dependent typical collapse mass M_c .

The baryon density Ω_b will naturally impact galaxy formation and the resulting SHMR. The baryon fraction in halos is expected to be roughly 90% of the universal value Ω_b/Ω_m and to be fairly independent of redshift up to $z = 1$, and halo mass above $\log M_h \approx 10.5$ (Crain et al. 2007). Given this independence we would expect a change in Ω_b at fixed Ω_m to change the normalization of the central and satellite SHMR. This effect will enter our formalism through shifts in M_{\min} , M_1 , and $f_{\text{cen},0}$. The parameter $\sigma_{\log M}$ is tied to the scatter in the SHMR and is therefore not effected by shifts in its normalization. In the top right panel of Fig. 4 we see that M_{\min} is set by the magnitude cuts, $f_{\text{cen},0}$ is set by the size cuts and M_1 is controlled by both magnitude and size cuts. By the same logic we would expect shifts in Ω_m at fixed Ω_b to produce shifts in M_{\min} , M_1 and $f_{\text{cen},0}$.

The key halo-model ingredient to predict the satellite occupation is the subhalo-mass-function (SHMF) and satellite SHMR. As previously mentioned shifts in Ω_m and Ω_b are expected to impact the normalization of the satellite SHMR, and therefore M_1 . Changes in the shape of the SHMF could potentially impact α . Recently Ragagnin et al. (2023) investigated the cosmological dependence of the satellite galaxy abundance in the *Magneticum* hydrodynamical simulations. They find that the normalization of the satellite abundance function, i.e. M_1 , depends weakly on cosmology parameters

particularly Ω_m and Ω_b . They also find that the logarithmic slope of the satellite occupation is insensitive to cosmology. This would suggest that we can safely treat the cosmological dependence of α as negligible. These arguments suggest that the functional form of our source HOD is insensitive to cosmology.

We have assumed that the HOD depends only on mass and can therefore be predicted with knowledge of the SHMR and SHMF, implicitly assuming a lack of galaxy assembly bias. Fortunately this is a safe assumption as Contreras et al. (2021) recently investigated the cosmological dependence of halo and galaxy assembly bias and found it to be “practically negligible”.

5. CONCLUSIONS

In this paper we have studied the galaxy-halo connection of DES-Y3 source galaxies in order to enable a future “lens equal source” analysis that includes small scales. We have developed a novel matching technique that takes advantage of the tight relation between the stellar mass and photometry of quenched and star-forming galaxies. This technique is applicable to any galaxy sample selected with photometry included in the 30 bands of COSMOS/UltraVISTA data.

Our study has revealed a complex phenomenology in the DES-Y3 source galaxy-halo connection that is not captured by standard HOD forms. In particular, our mocks indicate that DES-Y3 source galaxies suffer from significant central incompleteness, primarily driven by the size cuts that define the source sample. Additionally, we also observe this incompleteness to be strongly redshift and mass dependent. Indeed, we observe significant redshift evolution of both the central and satellite occupations of source galaxies over the redshift range $z = 0.1-1.25$.

We also observe the presence of central galaxy assembly bias in our mock source galaxies, with high- v_{max} halos being more likely to host source centrals than their low- v_{max} counterparts at fixed mass. To describe this behavior, we have developed an analytic form for the source HOD. We have shown that this analytic HOD form can describe the complex behavior of the source HOD across a wide range of redshifts, in particular the non-trivial central incompleteness introduced by source selection on galaxy sizes.

This halo-model approach allows us to convert our knowledge of galaxy formation and observable errors in DES photometry into priors on the HOD of source galaxies that can be used in future analyses. To define these HOD priors we have generated different realizations of our source HOD assuming realistic variations in photometry and the galaxy size-mass relation, and we

marginalize over the UNIVERSEMACHINE posterior. We fit each of these realizations using our new analytic form, confirming its suitability for modeling the source HOD. The dispersion in these best fit parameters then represents our uncertainty on the source sample’s galaxy-halo connection.

We have also used this set of realizations to train an emulator that models the dependence of the source HOD on redshift, errors in photometry and sizes as well as UNIVERSEMACHINE’s uncertainty on the stellar mass function. This emulator describes this behavior at the 1-3% level across the relevant mass and redshift ranges. This emulator allows us to convert prior knowledge on DES observational uncertainties into implicit priors on the source HOD. In the future, this kind of forward modeling approach can be used to integrate HOD models into likelihood analyses directly, independent of any functional form.

The principal challenge when trying to utilize information on small scales in clustering and galaxy-galaxy lensing is that the potential information gain is prohibited by model uncertainty. This model uncertainty does not only originate from a sufficiently flexible parameterization, but also from the lack of priors on the relevant parameters. In this work we have studied the halo-galaxy connection of DES-Y3 source galaxies and developed techniques to set robust and informative priors on their HOD. This halo-model approach enables us to

push to small scales and allows us to incorporate prior knowledge on galaxy formation physics to constrain nuisance parameters associated with the galaxy-halo connection. These techniques represent a powerful path towards maximizing the information gain from current and future galaxy surveys and will allow us to take advantage of future developments in our understanding of galaxy formation in a cosmological context.

ACKNOWLEDGEMENTS

We thank Andrew Hearin, Matthew Becker, ChangHoon Hahn, David Weinberg and Elisabeth Krause for valuable conversations on this work. AS, and TE are supported by the Department of Energy grant DE-SC0020215. Simulations in this paper use High Performance Computing (HPC) resources supported by the University of Arizona TRIF, UITS, and RDI and maintained by the UA Research Technologies department. Simulations were analyzed in part on computational resources of the Ohio Supercomputer Center ([Ohio Supercomputer Center 1987](#)), with resources supported in part by the Center for Cosmology and AstroParticle Physics at the Ohio State University. We gratefully acknowledge the use of the MATPLOTLIB software package ([Hunter 2007](#)) and the GNU Scientific library ([Galassi et al. 2009](#)). This research has made use of the SAO/NASA Astrophysics Data System.

REFERENCES

- Abbott, T. M. C., Abdalla, F. B., Alarcon, A., et al. 2018, *PhRvD*, 98, 043526, doi: [10.1103/PhysRevD.98.043526](https://doi.org/10.1103/PhysRevD.98.043526)
- Abbott, T. M. C., Aguena, M., Alarcon, A., et al. 2022, *PhRvD*, 105, 023520, doi: [10.1103/PhysRevD.105.023520](https://doi.org/10.1103/PhysRevD.105.023520)
- Akeson, R., Armus, L., Bachelet, E., et al. 2019, arXiv e-prints, arXiv:1902.05569. <https://arxiv.org/abs/1902.05569>
- Behroozi, P., Wechsler, R. H., Hearin, A. P., & Conroy, C. 2019, *MNRAS*, 488, 3143, doi: [10.1093/mnras/stz1182](https://doi.org/10.1093/mnras/stz1182)
- Berlind, A. A., & Weinberg, D. H. 2002, *ApJ*, 575, 587, doi: [10.1086/341469](https://doi.org/10.1086/341469)
- Brammer, G. B., van Dokkum, P. G., & Coppi, P. 2008, *ApJ*, 686, 1503, doi: [10.1086/591786](https://doi.org/10.1086/591786)
- Bruzual, G., & Charlot, S. 2003, *MNRAS*, 344, 1000, doi: [10.1046/j.1365-8711.2003.06897.x](https://doi.org/10.1046/j.1365-8711.2003.06897.x)
- Bryan, G. L., & Norman, M. L. 1998, *ApJ*, 495, 80, doi: [10.1086/305262](https://doi.org/10.1086/305262)
- Cacciato, M., Lahav, O., van den Bosch, F. C., Hoekstra, H., & Dekel, A. 2012, *MNRAS*, 426, 566, doi: [10.1111/j.1365-2966.2012.21762.x](https://doi.org/10.1111/j.1365-2966.2012.21762.x)
- Cacciato, M., van den Bosch, F. C., More, S., et al. 2009, *MNRAS*, 394, 929, doi: [10.1111/j.1365-2966.2008.14362.x](https://doi.org/10.1111/j.1365-2966.2008.14362.x)
- Cacciato, M., van den Bosch, F. C., More, S., Mo, H., & Yang, X. 2013, *MNRAS*, 430, 767, doi: [10.1093/mnras/sts525](https://doi.org/10.1093/mnras/sts525)
- Capak, P., Aussel, H., Ajiki, M., et al. 2007, *ApJS*, 172, 99, doi: [10.1086/519081](https://doi.org/10.1086/519081)
- Contreras, S., Chaves-Montero, J., Zennaro, M., & Angulo, R. E. 2021, *MNRAS*, 507, 3412, doi: [10.1093/mnras/stab2367](https://doi.org/10.1093/mnras/stab2367)
- Crain, R. A., Eke, V. R., Frenk, C. S., et al. 2007, *MNRAS*, 377, 41, doi: [10.1111/j.1365-2966.2007.11598.x](https://doi.org/10.1111/j.1365-2966.2007.11598.x)
- Croton, D. J., Gao, L., & White, S. D. M. 2007, *MNRAS*, 374, 1303, doi: [10.1111/j.1365-2966.2006.11230.x](https://doi.org/10.1111/j.1365-2966.2006.11230.x)
- DES Collaboration, Abbott, T. M. C., Aguena, M., et al. 2021, arXiv e-prints, arXiv:2105.13549. <https://arxiv.org/abs/2105.13549>
- DESI Collaboration, Aghamousa, A., Aguilar, J., et al. 2016, arXiv e-prints, arXiv:1611.00036. <https://arxiv.org/abs/1611.00036>

- Desjacques, V., Jeong, D., & Schmidt, F. 2018, *PhR*, 733, 1, doi: [10.1016/j.physrep.2017.12.002](https://doi.org/10.1016/j.physrep.2017.12.002)
- Doré, O., Bock, J., Ashby, M., et al. 2014, arXiv e-prints, arXiv:1412.4872. <https://arxiv.org/abs/1412.4872>
- Faltenbacher, A., & White, S. D. M. 2010, *ApJ*, 708, 469, doi: [10.1088/0004-637X/708/1/469](https://doi.org/10.1088/0004-637X/708/1/469)
- Fang, X., Eifler, T., Schaan, E., et al. 2022, *MNRAS*, 509, 5721, doi: [10.1093/mnras/stab3410](https://doi.org/10.1093/mnras/stab3410)
- Galassi, M., Davies, J., Theiler, J., et al. 2009, GNU Scientific Library Reference Manual, 3rd edn.
- Gao, L., Springel, V., & White, S. D. M. 2005, *MNRAS*, 363, L66, doi: [10.1111/j.1745-3933.2005.00084.x](https://doi.org/10.1111/j.1745-3933.2005.00084.x)
- Gao, L., & White, S. D. M. 2007, *MNRAS*, 377, L5, doi: [10.1111/j.1745-3933.2007.00292.x](https://doi.org/10.1111/j.1745-3933.2007.00292.x)
- Gatti, M., Sheldon, E., Amon, A., et al. 2021, *MNRAS*, 504, 4312, doi: [10.1093/mnras/stab918](https://doi.org/10.1093/mnras/stab918)
- Hadzhiyska, B., García-García, C., Alonso, D., Nicola, A., & Slosar, A. 2021, *JCAP*, 2021, 020, doi: [10.1088/1475-7516/2021/09/020](https://doi.org/10.1088/1475-7516/2021/09/020)
- Harker, G., Cole, S., Helly, J., Frenk, C., & Jenkins, A. 2006, *MNRAS*, 367, 1039, doi: [10.1111/j.1365-2966.2006.10022.x](https://doi.org/10.1111/j.1365-2966.2006.10022.x)
- Heymans, C., Tröster, T., Asgari, M., et al. 2021, *A&A*, 646, A140, doi: [10.1051/0004-6361/202039063](https://doi.org/10.1051/0004-6361/202039063)
- Hikage, C., Oguri, M., Hamana, T., et al. 2019, *PASJ*, 71, 43, doi: [10.1093/pasj/psz010](https://doi.org/10.1093/pasj/psz010)
- Hildebrandt, H., Viola, M., Heymans, C., et al. 2017, *MNRAS*, 465, 1454, doi: [10.1093/mnras/stw2805](https://doi.org/10.1093/mnras/stw2805)
- Huff, E., & Mandelbaum, R. 2017, arXiv e-prints, arXiv:1702.02600. <https://arxiv.org/abs/1702.02600>
- Hunter, J. D. 2007, *Computing In Science & Engineering*, 9, 90, doi: [10.1109/MCSE.2007.55](https://doi.org/10.1109/MCSE.2007.55)
- Ichikawa, T., Kajisawa, M., & Akhlaghi, M. 2012, *MNRAS*, 422, 1014, doi: [10.1111/j.1365-2966.2012.20674.x](https://doi.org/10.1111/j.1365-2966.2012.20674.x)
- Ivezić, Ž., Kahn, S. M., Tyson, J. A., et al. 2019, *ApJ*, 873, 111, doi: [10.3847/1538-4357/ab042c](https://doi.org/10.3847/1538-4357/ab042c)
- Jing, Y. P., Suto, Y., & Mo, H. J. 2007, *ApJ*, 657, 664, doi: [10.1086/511130](https://doi.org/10.1086/511130)
- Johnson, J. W., Maller, A. H., Berlind, A. A., Sinha, M., & Holley-Bockelmann, J. K. 2019, *MNRAS*, 486, 1156, doi: [10.1093/mnras/stz942](https://doi.org/10.1093/mnras/stz942)
- Kaiser, N. 1984, *ApJL*, 284, L9, doi: [10.1086/184341](https://doi.org/10.1086/184341)
- Klypin, A., Yepes, G., Gottlöber, S., Prada, F., & Heß, S. 2016, *MNRAS*, 457, 4340, doi: [10.1093/mnras/stw248](https://doi.org/10.1093/mnras/stw248)
- Kokron, N., DeRose, J., Chen, S.-F., White, M., & Wechsler, R. H. 2021, *MNRAS*, 505, 1422, doi: [10.1093/mnras/stab1358](https://doi.org/10.1093/mnras/stab1358)
- Krause, E., Fang, X., Pandey, S., et al. 2021, arXiv e-prints, arXiv:2105.13548, doi: [10.48550/arXiv.2105.13548](https://doi.org/10.48550/arXiv.2105.13548)
- Laureijs, R., Amiaux, J., Arduini, S., et al. 2011, arXiv e-prints, arXiv:1110.3193. <https://arxiv.org/abs/1110.3193>
- Leauthaud, A., Tinker, J., Behroozi, P. S., Busha, M. T., & Wechsler, R. H. 2011, *ApJ*, 738, 45, doi: [10.1088/0004-637X/738/1/45](https://doi.org/10.1088/0004-637X/738/1/45)
- Li, Y., Mo, H. J., & Gao, L. 2008, *MNRAS*, 389, 1419, doi: [10.1111/j.1365-2966.2008.13667.x](https://doi.org/10.1111/j.1365-2966.2008.13667.x)
- Mao, Y.-Y., Zentner, A. R., & Wechsler, R. H. 2018, *MNRAS*, 474, 5143, doi: [10.1093/mnras/stx3111](https://doi.org/10.1093/mnras/stx3111)
- Maraston, C. 2005, *MNRAS*, 362, 799, doi: [10.1111/j.1365-2966.2005.09270.x](https://doi.org/10.1111/j.1365-2966.2005.09270.x)
- Martin, D. C., Fanson, J., Schiminovich, D., et al. 2005, *ApJL*, 619, L1, doi: [10.1086/426387](https://doi.org/10.1086/426387)
- McCarthy, K. S., Zheng, Z., & Guo, H. 2019, *MNRAS*, 487, 2424, doi: [10.1093/mnras/stz1461](https://doi.org/10.1093/mnras/stz1461)
- McCracken, H. J., Milvang-Jensen, B., Dunlop, J., et al. 2012, *A&A*, 544, A156, doi: [10.1051/0004-6361/201219507](https://doi.org/10.1051/0004-6361/201219507)
- Miyatake, H., Kobayashi, Y., Takada, M., et al. 2022, *PhRvD*, 106, 083519, doi: [10.1103/PhysRevD.106.083519](https://doi.org/10.1103/PhysRevD.106.083519)
- Miyatake, H., Sugiyama, S., Takada, M., et al. 2023, arXiv e-prints, arXiv:2304.00704, doi: [10.48550/arXiv.2304.00704](https://doi.org/10.48550/arXiv.2304.00704)
- Modi, C., Chen, S.-F., & White, M. 2020, *MNRAS*, 492, 5754, doi: [10.1093/mnras/staa251](https://doi.org/10.1093/mnras/staa251)
- More, S., Miyatake, H., Mandelbaum, R., et al. 2015, *ApJ*, 806, 2, doi: [10.1088/0004-637X/806/1/2](https://doi.org/10.1088/0004-637X/806/1/2)
- More, S., van den Bosch, F. C., Cacciato, M., et al. 2013, *MNRAS*, 430, 747, doi: [10.1093/mnras/sts697](https://doi.org/10.1093/mnras/sts697)
- Mowla, L., van der Wel, A., van Dokkum, P., & Miller, T. B. 2019a, *ApJL*, 872, L13, doi: [10.3847/2041-8213/ab0379](https://doi.org/10.3847/2041-8213/ab0379)
- Mowla, L. A., van Dokkum, P., Brammer, G. B., et al. 2019b, *ApJ*, 880, 57, doi: [10.3847/1538-4357/ab290a](https://doi.org/10.3847/1538-4357/ab290a)
- Muzzin, A., Marchesini, D., Stefanon, M., et al. 2013a, *ApJS*, 206, 8, doi: [10.1088/0067-0049/206/1/8](https://doi.org/10.1088/0067-0049/206/1/8)
- . 2013b, *ApJ*, 777, 18, doi: [10.1088/0004-637X/777/1/18](https://doi.org/10.1088/0004-637X/777/1/18)
- Ohio Supercomputer Center. 1987, Ohio Supercomputer Center, <http://osc.edu/ark:/19495/f5s1ph73>
- Pandey, S., Krause, E., DeRose, J., et al. 2022, *PhRvD*, 106, 043520, doi: [10.1103/PhysRevD.106.043520](https://doi.org/10.1103/PhysRevD.106.043520)
- Planck Collaboration, Ade, P. A. R., Aghanim, N., et al. 2016, *A&A*, 594, A13, doi: [10.1051/0004-6361/201525830](https://doi.org/10.1051/0004-6361/201525830)
- Ragagnin, A., Fumagalli, A., Castro, T., et al. 2023, *A&A*, 675, A77, doi: [10.1051/0004-6361/202142392](https://doi.org/10.1051/0004-6361/202142392)
- Salcedo, A. N., Maller, A. H., Berlind, A. A., et al. 2018, *MNRAS*, 475, 4411, doi: [10.1093/mnras/sty109](https://doi.org/10.1093/mnras/sty109)

- Salcedo, A. N., Zu, Y., Zhang, Y., et al. 2022, *Science China Physics, Mechanics, and Astronomy*, 65, 109811, doi: [10.1007/s11433-022-1955-7](https://doi.org/10.1007/s11433-022-1955-7)
- Sanders, D. B., Salvato, M., Aussel, H., et al. 2007, *ApJS*, 172, 86, doi: [10.1086/517885](https://doi.org/10.1086/517885)
- Sato-Polito, G., Montero-Dorta, A. D., Abramo, L. R., Prada, F., & Klypin, A. 2019, *MNRAS*, 487, 1570, doi: [10.1093/mnras/stz1338](https://doi.org/10.1093/mnras/stz1338)
- Schaan, E., Ferraro, S., & Seljak, U. 2020, *JCAP*, 2020, 001, doi: [10.1088/1475-7516/2020/12/001](https://doi.org/10.1088/1475-7516/2020/12/001)
- Sheldon, E. S., & Huff, E. M. 2017, *ApJ*, 841, 24, doi: [10.3847/1538-4357/aa704b](https://doi.org/10.3847/1538-4357/aa704b)
- Sheth, R. K., & Tormen, G. 2004, *MNRAS*, 350, 1385, doi: [10.1111/j.1365-2966.2004.07733.x](https://doi.org/10.1111/j.1365-2966.2004.07733.x)
- Somerville, R. S., & Davé, R. 2015, *ARA&A*, 53, 51, doi: [10.1146/annurev-astro-082812-140951](https://doi.org/10.1146/annurev-astro-082812-140951)
- Sugiyama, S., Miyatake, H., More, S., et al. 2023, arXiv e-prints, arXiv:2304.00705, doi: [10.48550/arXiv.2304.00705](https://doi.org/10.48550/arXiv.2304.00705)
- van den Bosch, F. C., More, S., Cacciato, M., Mo, H., & Yang, X. 2013, *MNRAS*, 430, 725, doi: [10.1093/mnras/sts006](https://doi.org/10.1093/mnras/sts006)
- van der Wel, A., Franx, M., van Dokkum, P. G., et al. 2014, *ApJ*, 788, 28, doi: [10.1088/0004-637X/788/1/28](https://doi.org/10.1088/0004-637X/788/1/28)
- Wang, H. Y., Mo, H. J., & Jing, Y. P. 2007, *MNRAS*, 375, 633, doi: [10.1111/j.1365-2966.2006.11316.x](https://doi.org/10.1111/j.1365-2966.2006.11316.x)
- Wang, K., Mao, Y.-Y., Zentner, A. R., et al. 2022, *MNRAS*, 516, 4003, doi: [10.1093/mnras/stac2465](https://doi.org/10.1093/mnras/stac2465)
- Wechsler, R. H., Zentner, A. R., Bullock, J. S., Kravtsov, A. V., & Allgood, B. 2006, *ApJ*, 652, 71, doi: [10.1086/507120](https://doi.org/10.1086/507120)
- Williams, R. J., Quadri, R. F., Franx, M., van Dokkum, P., & Labbé, I. 2009, *ApJ*, 691, 1879, doi: [10.1088/0004-637X/691/2/1879](https://doi.org/10.1088/0004-637X/691/2/1879)
- Xu, X., & Zheng, Z. 2018, *MNRAS*, 479, 1579, doi: [10.1093/mnras/sty1547](https://doi.org/10.1093/mnras/sty1547)
- Yoo, J., & Seljak, U. 2012, *PhRvD*, 86, 083504, doi: [10.1103/PhysRevD.86.083504](https://doi.org/10.1103/PhysRevD.86.083504)
- Yoo, J., Tinker, J. L., Weinberg, D. H., et al. 2006, *ApJ*, 652, 26, doi: [10.1086/507591](https://doi.org/10.1086/507591)
- Zehavi, I., Zheng, Z., Weinberg, D. H., et al. 2005, *ApJ*, 630, 1, doi: [10.1086/431891](https://doi.org/10.1086/431891)
- Zennaro, M., Angulo, R. E., Pellejero-Ibáñez, M., et al. 2023, *MNRAS*, 524, 2407, doi: [10.1093/mnras/stad2008](https://doi.org/10.1093/mnras/stad2008)
- Zentner, A. R., Hearin, A., van den Bosch, F. C., Lange, J. U., & Villarreal, A. 2019, *MNRAS*, 485, 1196, doi: [10.1093/mnras/stz470](https://doi.org/10.1093/mnras/stz470)
- Zentner, A. R., Hearin, A. P., & van den Bosch, F. C. 2014, *MNRAS*, 443, 3044, doi: [10.1093/mnras/stu1383](https://doi.org/10.1093/mnras/stu1383)
- Zheng, Z., & Weinberg, D. H. 2007, *ApJ*, 659, 1, doi: [10.1086/512151](https://doi.org/10.1086/512151)
- Zheng, Z., Berlind, A. A., Weinberg, D. H., et al. 2005, *ApJ*, 633, 791, doi: [10.1086/466510](https://doi.org/10.1086/466510)
- Zu, Y., Zheng, Z., Zhu, G., & Jing, Y. P. 2008, *ApJ*, 686, 41, doi: [10.1086/591071](https://doi.org/10.1086/591071)